NASA Technical Paper 1328

The Effects of Curvature and Viscosity on Baroclinic Instability - A Two-Layer Model

William W. Fowlis and Salvador Arias

SEPTEMBER 1978

NASA

NASA Technical Paper 1328

The Effects of Curvature and Viscosity on Baroclinic Instability - A Two-Layer Model

William W. Fowlis and Salvador Arias
George C. Marshall Space Flight Center
Marshall Space Flight Center, Alabama

National Aeronautics
and Space Administration

**Scientific and Technical
Information Office**

1978

TABLE OF CONTENTS

LIST OF ILLUSTRATIONS

LIST OF ILLUSTRATIONS (Concluded)

THE EFFECTS OF CURVATURE AND VISCOSITY ON BAROCLINIC INSTABILITY – A TWO-LAYER MODEL

I. INTRODUCTION

The near-zero gravity environment of Spacelab presents an opportunity to perform geophysical fluid flow model experiments in true spherical geometry. A dominant radial dielectric body force, which is analogous to gravity, can be achieved over a volume of fluid held between two concentric spheres by applying a large voltage across the spheres [1,2]. There is no way such experiments can be performed in a laboratory on the Earth' s surface because the dielectric body force is weak and its effect is overwhelmed by terrestrial gravity.

A spherical model of the general circulation of the Earth' s atmosphere is being considered for Spacelab [2]. In the past, much sophisticated general circulation modeling has been performed in cylindrical geometries, and much has been learned which is relevant to the general circulation [3,4,5]. However, these models have serious limitations when attempts are made to extend their results to the spherical geometry of the atmosphere.

Systematic scaling of the governing equations for large-scale (synoptic-scale) processes in the atmosphere and the laboratory models yields an identical set of approximate equations for both systems known as the quasi-geostrophic equations [6] (except that curvature terms are missing from the cylindrical models); therefore, the laboratory experiments are called models. These equations do not include external heating processes which are important on longer time scales, and they do not include local dissipation processes which are small. Using the quasi-geostrophic equations, a linear stability analysis of a baroclinic zonal current contained between two rigid parallel boundaries has been completed. Some effects of curvature and boundary dissipation were included. The motivation for this analysis was to guide the design of the Atmospheric General Circulation Experiment (AGCE) for Spacelab. This report describes the stability analysis and presents the results. For additional information on AGCE and on baroclinic instability and the two-layer model, the reader is referred to the references herein.

No one has succeeded in solving analytically the equations for baroclinic instability on a sphere — they are not separable. To proceed, simplifications must be made. The analysis described in this report was performed on a β-plane. The β-plane is a tangent plane to a sphere at some latitude θ on which rectilinear cartesian coordinates are used and on which the variation of the local vertical component of rotation rate with latitude is represented linearly. The important effect of curvature introduced in this way is known as the β-effect. The effect of viscosity at the boundaries was introduced using the Ekman compatibility conditions [7]. These conditions enable one to omit a detailed discussion of the Ekman boundary layers on the horizontal surfaces while keeping the effect of these layers on the interior flow. No variation of the current in the north-south direction in the basic state was permitted. The continuous vertical structure was reduced to two layers within which all dependent quantities were kept constant. This two-layer model has been used by many workers and has proved to be a useful theoretical model for understanding baroclinic instability [6,8,9,10].

The analysis of the effect of Ekman damping on baroclinic waves on a β-plane, using a two-layer model, was first performed by Holopainen [11]. However, since Holopainen's formulation was for the atmosphere and his results were not presented in a form suitable for discussing the spherical model, it was necessary to repeat the analysis from the beginning. Holopainen discovered an unexpected destabilization of the waves by viscosity, which is discussed in Section V.

II. FORMULATION OF THE TWO-LAYER MODEL

Let us consider a β-plane on which the axes (x,y,z) correspond to eastward, northward and vertical directions, respectively. Let the corresponding velocity components be (u,v,w). The quasi-geostrophic set of equations on the β-plane is

$$\frac{\partial \zeta}{\partial t} + (\underline{v}_n \cdot \nabla)\zeta + \beta v_n = -f\nabla \cdot \underline{v}_d \quad , \tag{1}$$

$$\frac{1}{\rho}\nabla^2 p = -f\nabla \cdot (\underline{\hat{z}} \times \underline{v}_n) \quad , \tag{2}$$

$$\frac{\partial p}{\partial z} = -\rho g \quad , \tag{3}$$

$$\nabla \cdot \underline{v}_n + \frac{\partial w}{\partial z} = 0 \quad , \tag{4}$$

$$\frac{\partial T}{\partial t} + (\underline{v}_n \cdot \nabla) T + w \frac{\partial T}{\partial z} = 0 \quad , \tag{5}$$

$$\rho = \rho_0 \{ 1 - \alpha (T - T_0) \} \quad , \tag{6}$$

where

ζ = vertical component of relative vorticity

$\underline{v}_n$ = nondivergent part of the horizontal flow

$\underline{v}_d$ = divergent part of the horizontal flow

∇ = horizontal operator

$\hat{\underline{z}}$ = unit vector in the z-direction

p = pressure

T = temperature

ρ = density

g = gravity (or some other body force)

f = twice the vertical component of the rotation rate

$\beta = df/dy$.

For the derivation of these equations and for further discussion, see References 6 and 12.

Since $\nabla \cdot \underline{v}_n = 0$, we can write $\underline{v}_n$ in terms of a stream function ψ as

$$\underline{v}_n = \hat{\underline{z}} \times \nabla\psi \tag{7}$$

and

$$\zeta = \hat{\underline{z}} \cdot \nabla \times \underline{v}_n = \nabla^2\psi \quad . \tag{8}$$

Substituting from equations (7) and (8) into equations (1) and (2), we obtain

$$\frac{\partial}{\partial t}(\nabla^2\psi) + (\underline{v}_n \cdot \nabla)\nabla^2\psi + \beta v_n = -f\nabla \cdot \underline{v}_d \quad , \tag{9}$$

$$\frac{1}{\rho}\nabla^2 p = f\nabla^2\psi \quad . \tag{10}$$

Eliminating further and using equations (9) and (10) and (3) through (6), we obtain

$$\frac{\partial}{\partial t}(\nabla^2\psi) + (\underline{v}_n \cdot \nabla)\nabla^2\psi + \beta v_n = f\frac{\partial w}{\partial z} \quad , \tag{11}$$

$$\frac{\partial}{\partial t}\left(\frac{\partial\psi}{\partial z}\right) + (\underline{v}_n \cdot \nabla)\frac{\partial\psi}{\partial z} = -\frac{\chi}{f}w \quad , \tag{12}$$

where $\chi = g\alpha\dfrac{\partial T}{\partial z}$.

Equations (11) and (12) can be solved as they are with appropriate boundary conditions [13], but the solutions are in the form of confluent hypergeometric functions, and computations based on such functions with complex arguments require much time-consuming programming. A two-layer model is used.

In the two-layer model the fluid is divided into two layers bounded by surfaces, as shown in Figure 1. The surfaces at levels 0, 2, and 4 divide the fluid into the two layers. In each layer, the values of stream function and vertical velocity (and other dependent variables) are assumed constant throughout the layer and are set equal to their values at the midpoint of the layer. The midpoints are denoted by levels 1 and 3. The vorticity equation (11) is applied at levels 1 and 3 with $\partial w/\partial z$ evaluated as

$$\left(\frac{\partial w}{\partial z}\right)_1 = \frac{w_2 - w_0}{\Delta z} \quad , \tag{13a}$$

$$\left(\frac{\partial w}{\partial z}\right)_3 = \frac{w_4 - w_2}{\Delta z} \quad , \tag{13b}$$

where Δz is the thickness of each layer. The resulting vorticity equations are

$$\frac{\partial}{\partial t}\nabla^2\psi_1 + (\underline{v}_1 \cdot \nabla)\nabla^2\psi_1 + \beta v_1 = \frac{f}{\Delta z}(w_2 - w_0) \quad , \tag{14}$$

$$\frac{\partial}{\partial t}\nabla^2\psi_3 + (\underline{v}_3 \cdot \nabla)\nabla^2\psi_3 + \beta v_3 = \frac{f}{\Delta z}(w_4 - w_2) \quad . \tag{15}$$

Equation (12) is applied at level 2 as

$$\frac{\partial}{\partial t}(\psi_3 - \psi_1) + (\underline{v}_2 \cdot \nabla)(\psi_3 - \psi_1) = -\frac{\chi \Delta z}{f} w_2 \quad . \tag{16}$$

$\underline{v}_2$ is not a predicted quantity of the model, but is obtained by linear interpolation between levels 1 and 3,

$$\psi_2 = \frac{1}{2}(\psi_1 + \psi_3) \quad . \tag{17}$$

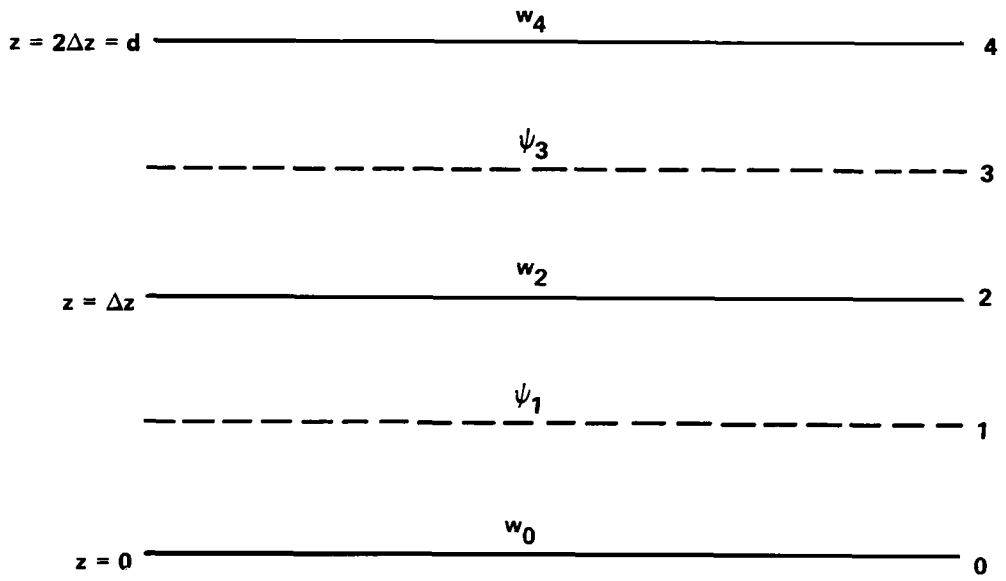

Figure 1. Arrangement of variables in the vertical for the two-layer model.

Therefore, remembering equations (7) and (17), equations (14), (15), and (16) make up three equations in the three unknowns ψ_1, ψ_3, and w_2. w_0 and w_4 are specified by the boundary conditions.

A. The Basic State

We shall perturb a geostrophic baroclinic steady state specified by:

$$v_1 = v_3 = 0 \quad , \quad w_0 = w_2 = w_4 = 0 \quad , \tag{18a}$$

$$u_1 = U_1 \quad , \quad u_3 = U_3 \quad , \tag{18b}$$

$$\psi_1 = -U_1 y \quad , \quad \psi_3 = -U_3 y \quad , \tag{18c}$$

$$U_T = \frac{1}{2}(U_3 - U_1) = -\frac{g\alpha}{f}\frac{dT_0}{dz}\Delta z \quad , \tag{18d}$$

where U_1 and U_3 are constant horizontal velocities in levels 1 and 3, respectively, U_T is the thermal wind, and $T_0(y,z)$ is the basic state temperature distribution. Equations (18) are steady solutions of equations (14), (15), and (16).

B. The Perturbed State

We now define perturbation quantities as follows:

$$\psi_1 = -U_1 y + \psi_1'(x,y,t) \quad , \tag{19a}$$

$$\psi_3 = -U_3 y + \psi_3'(x,y,t) \quad , \tag{19b}$$

$$w_2 = w_2'(x,y,t) \quad . \tag{19c}$$

The superfix denotes a perturbation quantity. Substituting from equation (19) into equations (14), (15), and (16) and linearizing by neglecting products of perturbation quantities, we obtain

$$\left(\frac{\partial}{\partial t} + U_1 \frac{\partial}{\partial x}\right)\left(\frac{\partial^2 \psi_1'}{\partial x^2} + \frac{\partial^2 \psi_1'}{\partial y^2}\right) + \beta \frac{\partial \psi_1'}{\partial x} = \frac{f}{\Delta z}(w_2' - w_0') \quad , \tag{20}$$

$$\left(\frac{\partial}{\partial t} + U_3 \frac{\partial}{\partial x}\right)\left(\frac{\partial^2 \psi_3'}{\partial x^2} + \frac{\partial^2 \psi_3'}{\partial y^2}\right) + \beta \frac{\partial \psi_3'}{\partial x} = \frac{f}{\Delta z}(w_4' - w_2') \quad , \tag{21}$$

$$\left(\frac{\partial}{\partial t} + U_m \frac{\partial}{\partial x}\right)(\psi_3' - \psi_1') - U_T \frac{\partial}{\partial x}(\psi_1' + \psi_3') = -\frac{\chi \Delta z}{f} w_2' \quad , \tag{22}$$

where $U_m = 1/2\,(U_1 + U_3)$.

Scaling shows that the direct effect of viscosity on the interior flow is weak, and hence viscous terms are not present in the quasi-geostrophic equations (1) through (6). The dissipative effect of viscosity enters this problem through the vertical velocity forced at the boundaries by convergence and divergence of the flow. These vertical velocities are given by the Ekman compatibility conditions, namely,

$$\text{at } z = 0 \quad , \quad w_0' = \frac{1}{2}\left(\frac{\nu}{\Omega}\right)^{1/2}\left(\frac{\partial^2 \psi_1'}{\partial x^2} + \frac{\partial^2 \psi_1'}{\partial y^2}\right) \quad , \tag{23a}$$

$$\text{at } z = d \quad , \quad w_4' = -\frac{1}{2}\left(\frac{\nu}{\Omega}\right)^{1/2}\left(\frac{\partial^2 \psi_3'}{\partial x^2} + \frac{\partial^2 \psi_3'}{\partial y^2}\right) \quad , \tag{23b}$$

where ν is the kinematic viscosity and Ω is the rotation rate ($f = 2\Omega$).

III. SOLUTION OF THE MODEL

The two-layer model stability problem is now completely formulated by equations (20), (21), and (22) and boundary conditions of equations (23). We assume solutions of the form

$$\psi_1' = A \exp i(\lambda x + \mu y - \lambda c t) \quad , \tag{24a}$$

$$\psi_3' = B \exp i(\lambda x + \mu y - \lambda c t) \quad , \tag{24b}$$

$$w_2' = C \exp i(\lambda y + \mu y - \lambda c t) \quad . \tag{24c}$$

Substituting equations (24) into equations (20), (21), and (22), we obtain

$$i\lambda\{(c - U_1)k^2 + \beta\} A = \frac{f}{\Delta z} (C - w_0') \quad , \tag{25}$$

$$i\lambda\{(c - U_3)k^2 + \beta\} B = \frac{f}{\Delta f} (w_4' - C) \quad , \tag{26}$$

$$-i\lambda(c - U_3) A + i\lambda(c - U_1) B = \frac{\chi \Delta z}{f} C \quad , \tag{27}$$

where $k^2 = \lambda^2 + \mu^2$ and $\chi = g\alpha \, dT_0/dz$.

We now proceed to apply the boundary conditions of equations (23). We obtain

$$i\lambda\{(c - U_1)k^2 + \beta + i\delta\} A - \frac{f}{\Delta z} C = 0 \quad , \tag{28}$$

$$i\lambda\{(c - U_3)k^2 + \beta + i\delta\} B + \frac{f}{\Delta z} C = 0 \quad , \tag{29}$$

$$-i\lambda(c - U_3) A + i\lambda(c - U_1) B - \frac{\chi \Delta z}{f} C = 0 \quad , \tag{30}$$

where $\delta = (fk^2/2\lambda\Delta z)(\nu/\Omega)^{1/2}$.

The condition for a nontrivial solution of equations (28) through (30) is

$$\begin{vmatrix} i\lambda\{(c - U_1)k^2 + \beta + i\delta\} & 0 & -\frac{f}{\Delta z} \\ 0 & i\lambda\{(c - U_3)k^2 + \beta + i\delta\} & \frac{f}{\Delta z} \\ -i\lambda(c - U_3) & i\lambda(c - U_1) & -\frac{\chi \Delta z}{f} \end{vmatrix} = 0 \quad . \tag{31}$$

Multiplying out, we have

$$i\lambda\{(c - U_1)k^2 + \beta + i\delta\}\left[i\lambda\{(c - U_3)k^2 + \beta + i\delta\}\left(-\frac{\chi\Delta z}{f}\right) - i\lambda(c - U_1)\left(\frac{f}{\Delta z}\right)\right]$$

$$-\left(\frac{f}{\Delta z}\right)[-\lambda^2(c - U_3)\{(c - U_3)k^2 + \beta + i\delta\}] = 0 \quad . \tag{32}$$

Rearranging equation (32) to give a polynomial in c, we obtain

$$k^2(k^2 + 2s^2)c^2 + \{2(k^2 + s^2)(\beta + i\delta) - (U_1 + U_3)k^2(k^2 + 2s^2)\}\ c + \{k^4U_1U_3$$

$$+ (\beta + i\delta)^2 - (U_1 + U_3)(k^2 + s^2)(\beta + i\delta) + k^2s^2(U_1^2 + U_3^2)\} = 0 \quad , \tag{33}$$

where $s^2 = f^2/\chi\Delta z^2$.

Solving equation (33) for c gives

$$c = U_m - (\beta + i\delta)\frac{(k^2 + s^2)}{k^2(k^2 + 2s^2)} \pm \frac{1}{k^2(k^2 + 2s^2)}\{(\beta + i\delta)^2s^4 + U_T^2k^4(k^4 - 4s^4)\}^{1/2} \quad . \tag{34}$$

Separating equation (34) into real and imaginary parts, we have

$$\mathcal{R}(c) = U_m - \beta\frac{(k^2 + s^2)}{k^2(k^2 + 2s^2)} \pm \frac{1}{k^2(k^2 + 2s^2)}[\{(\beta^2 - \delta^2)s^4 + U_T^2k^4(k^4 - 4s^4)\}^2$$

$$+ 4\beta^2\delta^2s^8]^{1/4}\cos\frac{\xi}{2} \quad , \tag{35}$$

$$\vartheta(c) = -\delta \frac{(k^2 + s^2)}{k^2(k^2 + 2s^2)} \pm \frac{1}{k^2(k^2 + 2s^2)} \left[\{(\beta^2 - \delta^2)s^4 + U_T{}^2k^4(k^4 - 4s^4) + 4\beta^2\delta^2s^8\right]^{1/4} \sin\frac{\xi}{2} \quad , \tag{36}$$

where

$$\tan\xi = \frac{2\beta\delta s^4}{(\beta^2 - \delta^2)s^4 + U_T{}^2k^4(k^4 - 4s^4)} \quad . \tag{37}$$

The condition for marginal stability is found by letting $\vartheta(c) = 0$. Using equations (36) and (37), we obtain

$$\beta^2s^4 + (k^2 + s^2)^2\delta^2 = -U_T{}^2k^2(k^2 - 2s^2)(k^2 + s^2)^2 \quad . \tag{38}$$

It is convenient to write equations (35), (36), and (38) in nondimensional form; these equations are, respectively,

$$\Re(c^*) = \frac{\sigma_R^*}{\lambda^*} = U_m^* - \frac{\epsilon B\left(k^{*2} + \frac{4}{S}\right)}{\Gamma_1 k^{*2}\left(k^{*2} + \frac{8}{S}\right)} \pm \frac{\epsilon S}{2\Gamma_1 k^{*2}\left(k^{*2} + \frac{8}{S}\right)} M^{1/4} \cos\frac{\xi}{2} \quad , \tag{40}$$

$$\vartheta(c^*) = \frac{\sigma_I^*}{\lambda^*} = -\frac{\sqrt{2}\epsilon\left(k^{*2} + \frac{4}{S}\right)}{\Gamma_1 Ta_m^{1/4}\lambda^*\left(k^{*2} + \frac{8}{S}\right)} \pm \frac{\epsilon S}{2\Gamma_1 k^{*2}\left(k^{*2} + \frac{8}{S}\right)} M^{1/4} \sin\frac{\xi}{2} \quad , \tag{41}$$

$$B^2 + \frac{2k^{*4}}{\lambda^{*2}} \left(Ta_m\right)^{-1/2} \left(1 + \frac{1}{4} k^{*2}S\right)^2 = 2k^{*2}S \left(1 + \frac{1}{4} k^{*2}S\right)^2 \left(1 - \frac{1}{8} k^{*2}S\right) \quad , \tag{42}$$

where σ_R^* is the angular frequency and σ_I^* is the growth rate and where,

$$M = \left\{ \left(B^2 - \frac{2k^{*4}}{\lambda^{*2}} Ta_m^{-1/2} \right) \frac{64}{S^4} + k^{*4} \left(k^{*4} - \frac{64}{S^2} \right) \right\}^2 + 16 \times 2048 \frac{k^{*4} B^2}{\lambda^{*2} Ta_m^{1/2} S^8} \quad , \tag{43}$$

$$\tan \xi = \frac{32 \sqrt{2}\, k^{*2} B}{\lambda^* Ta_m^{1/4} S^2 \left\{ \left(B^2 - \frac{2k^{*4}}{\lambda^{*2}} Ta_m^{-1/2} \right) \frac{16}{S^2} + \frac{k^{*4} S^2}{4} \left(k^{*4} - \frac{64}{S^2} \right) \right\}} \quad . \tag{44}$$

An asterisk denotes a nondimensional quantity; $B = \Gamma_1 \tan \phi / \Gamma_2 \epsilon$, $Ta_m = \epsilon^4 / \Gamma_1^4 E^2$, $S = g\alpha \Delta T_v / f^2 d$; $\Gamma_1 = h/d$, $\Gamma_2 = \bar{R}/d$, $\epsilon = \Delta T_h / \Delta T_d$, $E = \nu / fd^2$; and h is a horizontal scale, d is the depth, $\bar{R}$ is the mean radius, and ϕ is colatitude, ΔT_h is the imposed horizontal temperature difference of the basic state, and ΔT_d is the imposed vertical temperature difference of the basic state. k^* and λ^* are wave numbers nondimensionalized by d. U_m^* and c^* are nondimensionalized by fd. σ_R^* and σ_I^* are nondimensionalized by f.

IV. THE RESULTS

Before using equations (40), (41), and (42) to plot the results for ranges of the dimensionless parameters (ϵ, B, S, and Ta_m) and the wave numbers (λ^* and μ^*), we shall convert λ^* and μ^* to actual discrete zonal and meridional wave numbers for finite spherical geometry. Consider our β-plane at latitude θ on a sphere of mean radius $\bar{R}$; then,

$$\frac{2\pi}{\lambda} = \frac{2\pi\bar{R}\cos\theta}{m} \quad , \quad \text{i.e.,} \quad \lambda^* = \frac{m}{\Gamma_2 \cos\theta} \quad , \tag{45a}$$

where m is the actual discrete zonal wave number. If we assume that the wave fills the meridional scale h, we have

$$\frac{2\pi}{\mu} = 2h \quad ; \quad \text{i.e.,} \quad \mu^* = \frac{\pi}{h} \quad . \tag{45b}$$

We now proceed to plot the marginal stability diagrams using equation (42). Figures 2 through 11 show S versus Ta_m for several different values of m and for fixed values of ϵ, Γ_1, Γ_2, and B. Each figure also shows the results for B = 0. The fixed parameters are varied systematically as one proceeds from diagram to diagram. $\theta = 45°$ for all the figures. The Table presents a list of the figures and the corresponding values of the parameters.

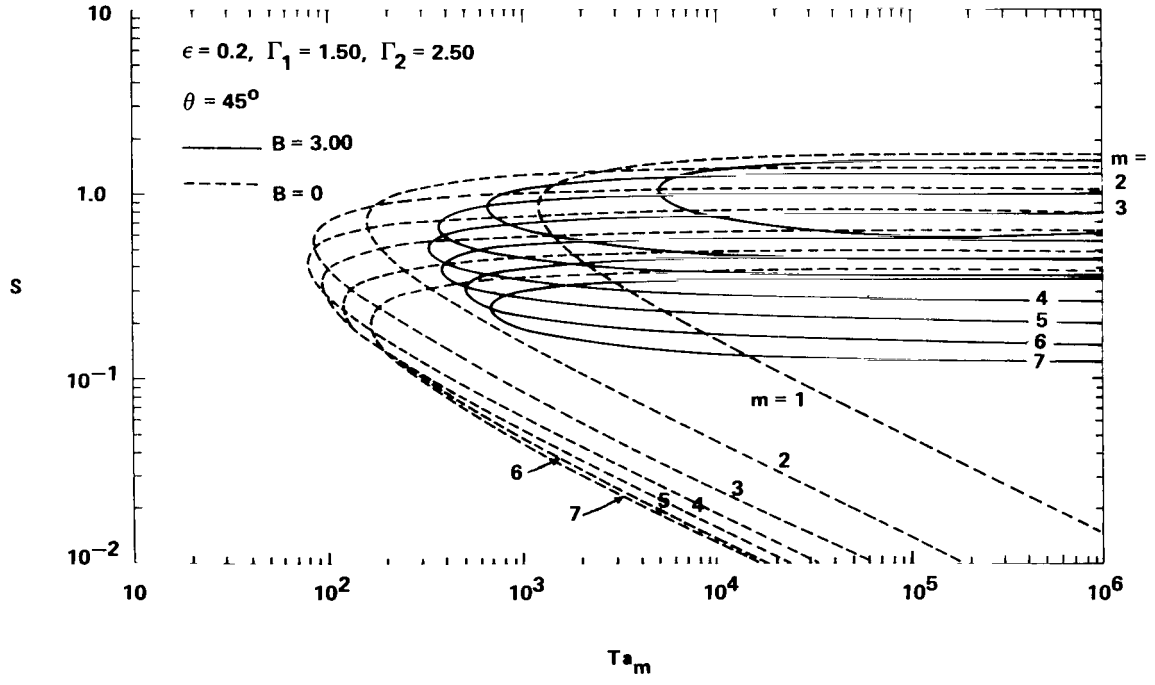

Figure 2. Plots of the marginal stability curves for different wave numbers (m) and for $\epsilon = 0.2$, $\Gamma_1 = 1.50$, and $\Gamma_2 = 2.50$ [the continuous curves are for B = 3.00 and the dashed curves are for zero curvature (B = 0)].

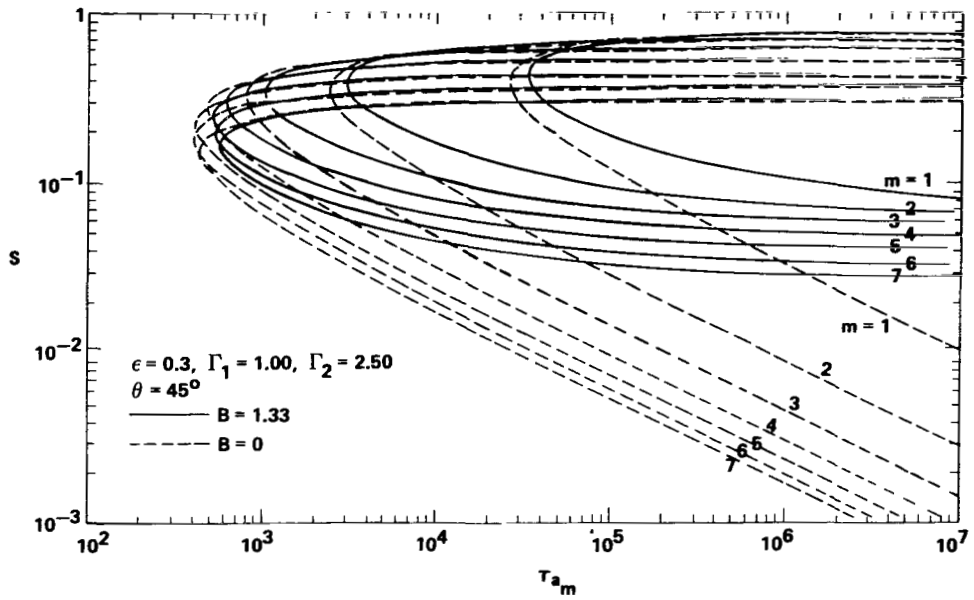

Figure 3. Plots of the marginal stability curves for different values of m and for $\epsilon = 0.3$, $\Gamma_1 = 1.00$, and $\Gamma_2 = 2.50$ (the continuous curves are for B = 1.33 and the dashed curves for B = 0).

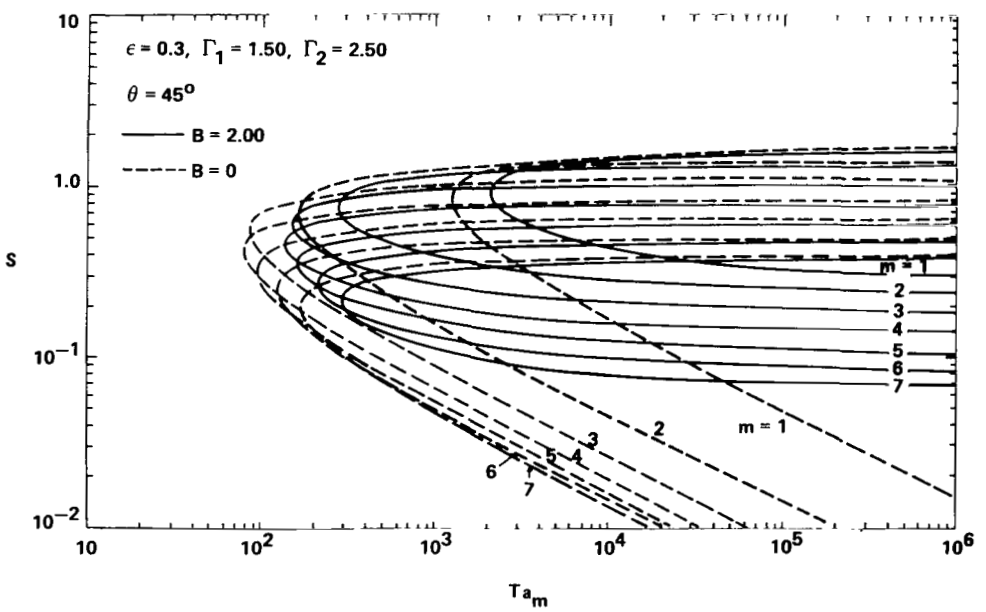

Figure 4. Plots of the marginal stability curves for different values of m and for $\epsilon = 0.3$, $\Gamma_1 = 1.50$, and $\Gamma_2 = 2.50$ (the continuous curves are for B = 2.00 and the dashed curves for B = 0).

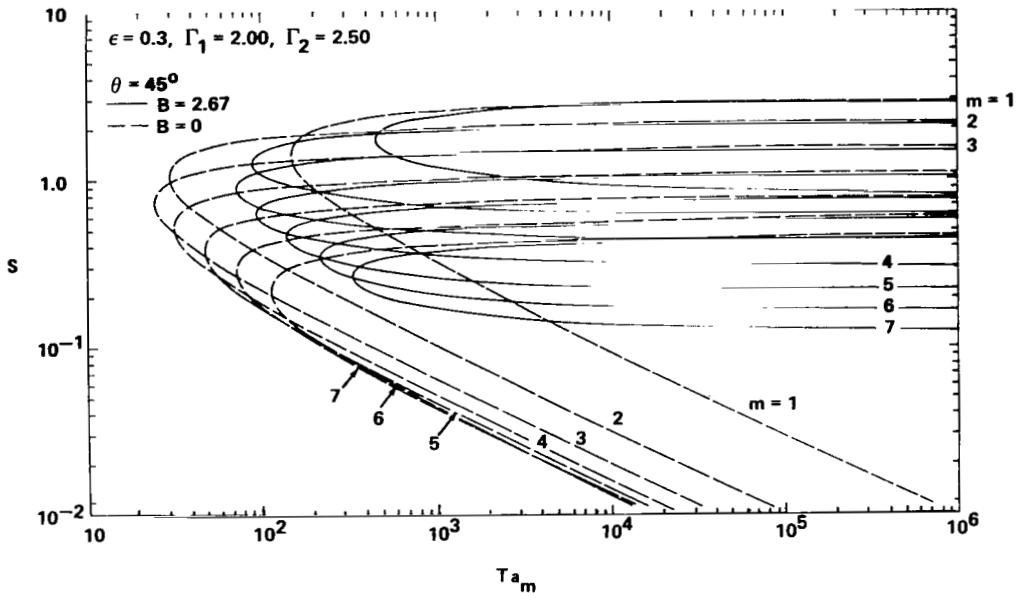

Figure 5. Plots of the marginal stability curves for different values of m and for $\epsilon = 0.3$, $\Gamma_1 = 2.00$, and $\Gamma_2 = 2.50$ (the continuous curves are for B = 2.67 and the dashed curves for B = 0).

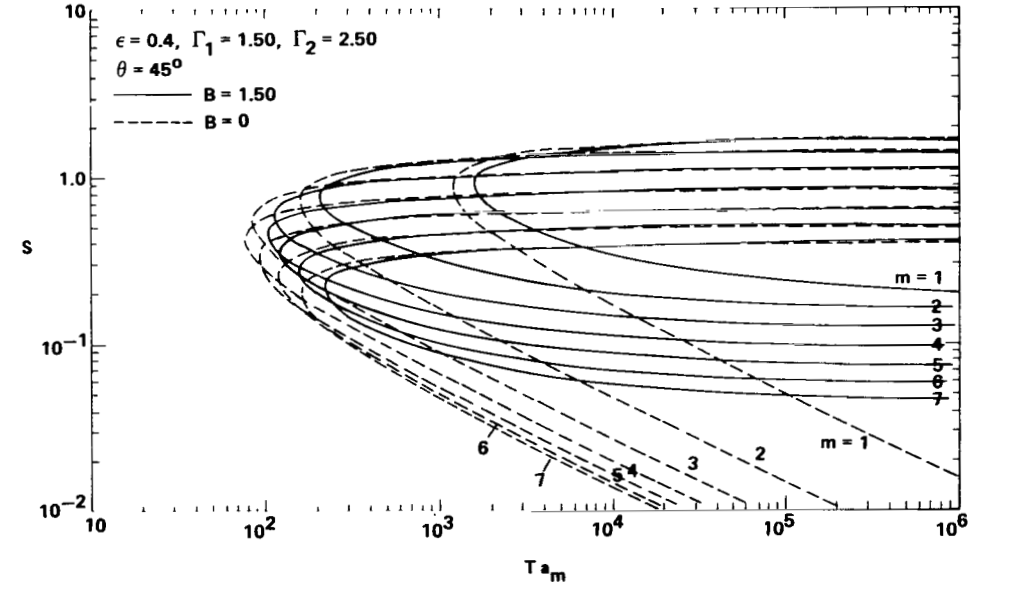

Figure 6. Plots of the marginal stability curves for different values of m and for $\epsilon = 0.4$, $\Gamma_1 = 1.50$, and $\Gamma_2 = 2.50$ (the continuous curves are for B = 1.50 and the dashed curves for B = 0).

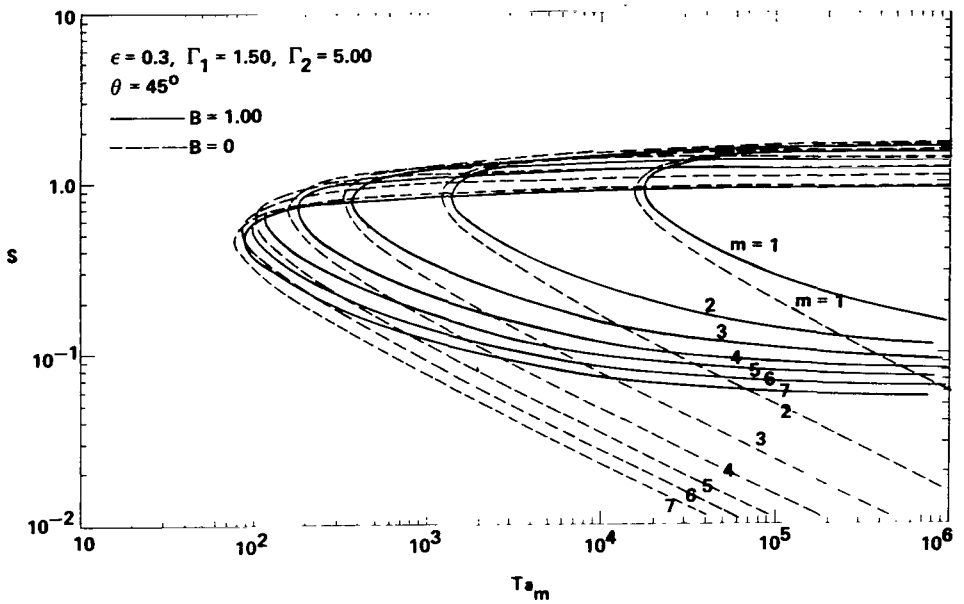

Figure 7. Plots of the marginal stability curves for different values of m and for $\epsilon = 0.3$, $\Gamma_1 = 1.50$, and $\Gamma_2 = 5.00$ (the continuous curves are for B = 1.00 and the dashed curves for B = 0).

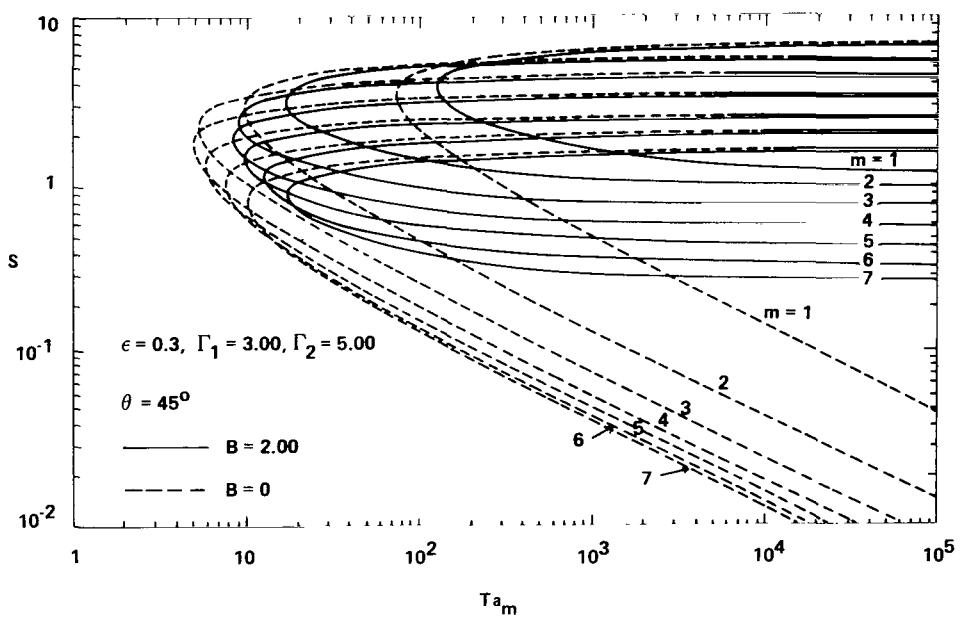

Figure 8. Plots of the marginal stability curves for different values of m and for $\epsilon = 0.3$, $\Gamma_1 = 3.00$, and $\Gamma_2 = 5.00$ (the continuous curves are for B = 2.00 and the dashed curves for B = 0).

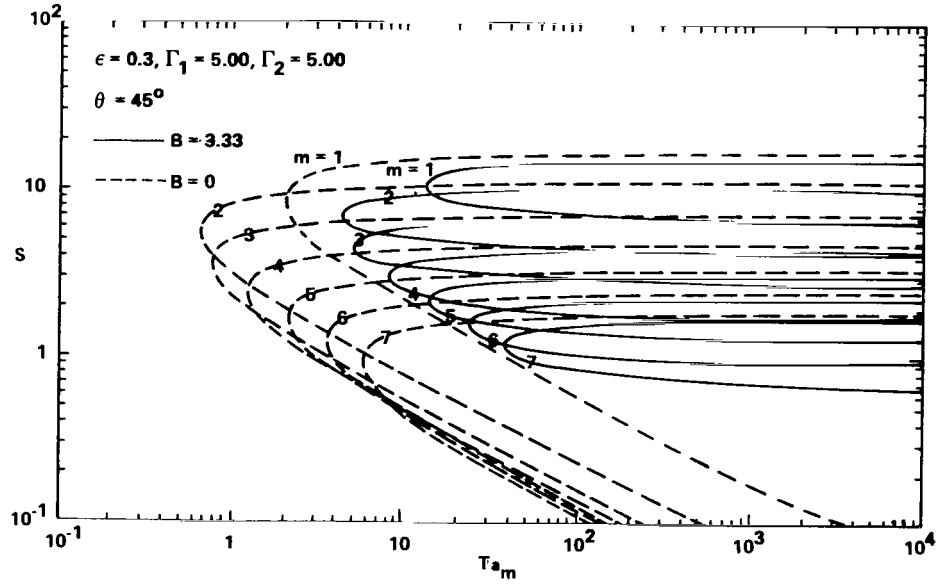

Figure 9. Plots of the marginal stability curves for different values of m and for $\epsilon = 0.3$, $\Gamma_1 = 5.00$, and $\Gamma_2 = 5.00$ (the continuous curves are for B = 3.33 and the dashed curves for B = 0).

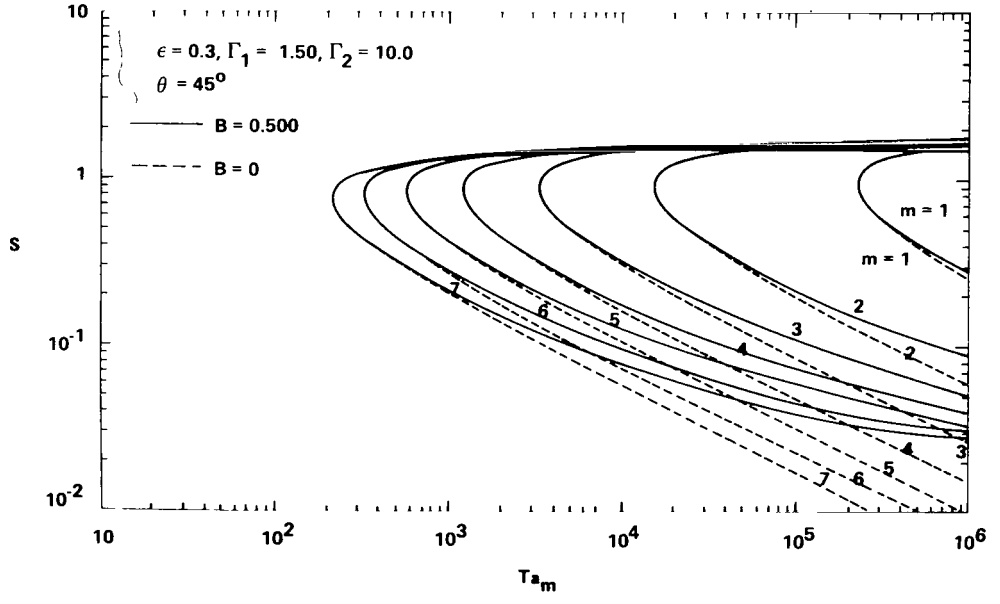

Figure 10. Plots of the marginal stability curves for different values of m and for $\epsilon = 0.3$, $\Gamma_1 = 1.50$, and $\Gamma_2 = 10.0$ (the continuous curves are for B = 0.50 and the dashed curves for B = 0).

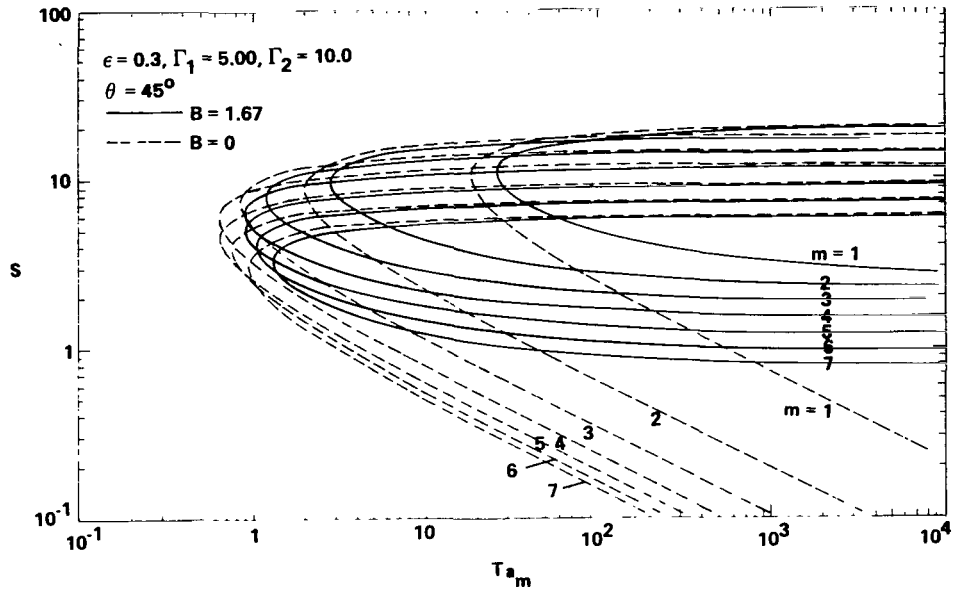

Figure 11. Plots of the marginal stability curves for different values of m and for $\epsilon = 0.3$, $\Gamma_1 = 5.00$, and $\Gamma_2 = 10.0$ (the continuous curves are for B = 1.67 and the dashed curves for B = 0).

TABLE. MARGINAL STABILITY CURVE PARAMETERS

Figure No.	ϵ	Γ_1	Γ_2	B
2	0.2	1.50	2.50	3.00
3	0.3	1.00	2.50	1.33
4	0.3	1.50	2.50	2.00
5	0.3	2.00	2.50	2.67
6	0.4	1.50	2.50	1.50
7	0.3	1.50	5.00	1.00
8	0.3	3.00	5.00	2.00
9	0.3	5.00	5.00	3.33
10	0.3	1.50	10.0	0.500
11	0.3	5.00	10.0	1.67

Figures 12 and 13 show the phase speeds (c_R^*) and growth rates (σ_I^*) plotted using equations (40) and (41), respectively. Figures 12 and 13 also show the ordinate plotted against m for different values of S. Both plots are for the conditions of Figure 8 ($\epsilon = 0.3$, $\Gamma_1 = 3.00$, $\Gamma_2 = 5.00$, $B = 2.00$) and for $Ta_m = 10^3$.

The stability diagrams can be plotted and discussed in several different ways. The plots chosen are those closest to the way in which the experimental annulus results were presented. Each figure should be considered as showing the results for varying ΔT_h and Ω only, and for fixed viscosity and geometry. Each plot assumes that ϵ is constant. In fact, ϵ is a dependent quantity, and its behavior should be determined by a complete solution of the basic state. This is a much more difficult problem than the one considered, but measurements from the annulus experiments show that ϵ is primarily a function of the geometry and is only weakly dependent on ΔT_h and Ω. S can be considered as a measure of the thermal driving force, Ta_m as a measure of damping, and B as a measure of curvature. Note that ϵ occurs in Ta_m and B.

The results show that the flow is unstable within a range of S for large values of Ta_m and moderate values of B. For small values of Ta_m, corresponding to large dissipation, the marginal stability curves form a knee to the left of which the flow is stable for all S. For large values of S the flow is stable even for asymptotically large Ta_m. This is a short wavelength cutoff, known as the Eady cutoff. In this model it is due to the fact that eventually the unstable wavelength is too long to fit into the finite geometry. For small values of S below the knee there is a long wavelength cutoff.

Note that increasing B from zero has at first almost no effect on the short wavelength cutoff but has a significant effect on the long wavelength cutoff. Even for relatively small B the effect of curvature is observed on the lower transition. When $B \geq 4$, the instability is completely suppressed.

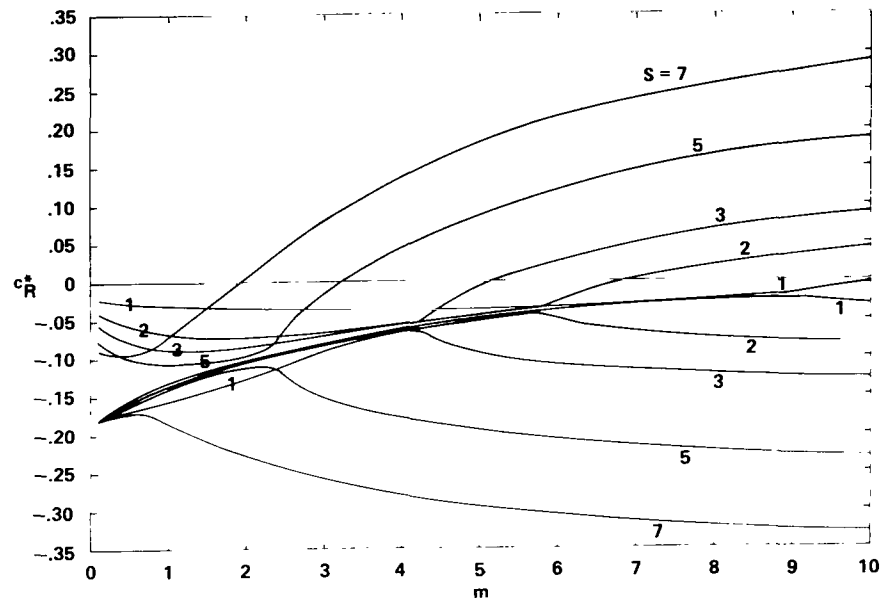

Figure 12. The phase speed (c_R^*) versus m for different values of S and for the conditions of Figure 8 ($\epsilon = 0.3$, $\Gamma_1 = 3.00$, $\Gamma_2 = 5.00$, $B = 2.00$) and for $Ta_m = 10^3$.

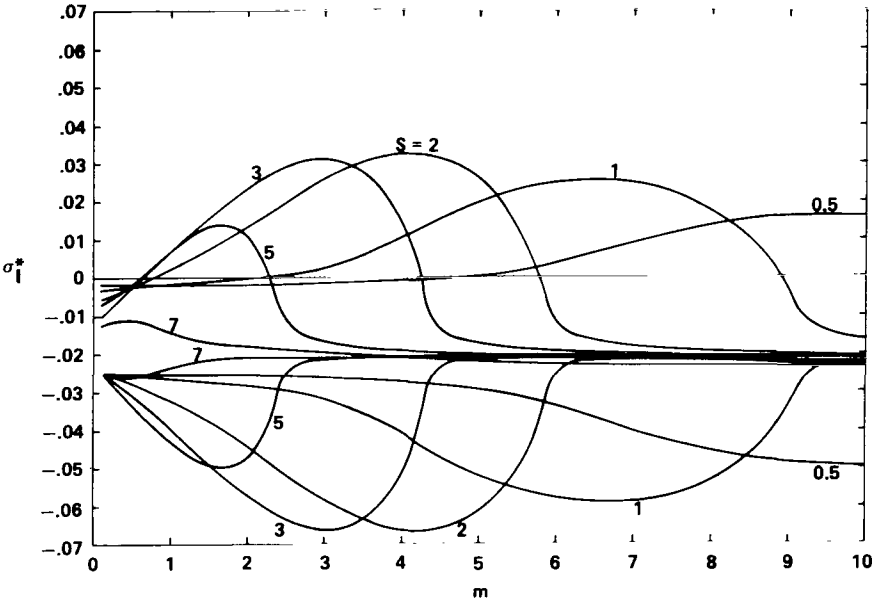

Figure 13. The growth rate (σ_I^*) versus m for different values of S and for the conditions of Figure 8 ($\epsilon = 0.3$, $\Gamma_1 = 3.00$, $\Gamma_2 = 5.00$, $B = 2.00$) and for $Ta_m = 10^3$.

V. SPECIAL CASES

We have performed a stability analysis in which curvature and dissipation are present. It is interesting to examine the following special cases: (1) both curvature and dissipation equal to zero ($B = 0$, $E = 0$); (2) curvature equal to zero, but dissipation not equal to zero ($B = 0$, $E \neq 0$); and (3) curvature not equal to zero, but dissipation equal to zero ($B \neq 0$, $E = 0$).

For $B = 0$ and $E = 0$ ($Ta_m = \infty$), the marginal stability criterion equation (42) reduces to

$$S = \frac{8}{k^{*2}} \quad . \tag{46}$$

This analysis was first performed for a continuous linear vertical shear model by Eady [14], who obtained the result

$$S = \frac{5.76}{k^{*2}} \quad . \tag{47}$$

Both results give a short wavelength cutoff only. We see that the two-layer model is in approximate quantitative agreement with the continuous model.

For $B = 0$ and $E \neq 0$, the criterion equation (42) reduces to

$$S\left(1 + \frac{8}{\lambda^{*2} Ta_m^{1/2} S^2}\right) = \frac{8}{k^{*2}} \quad . \tag{48}$$

This formula was used to plot the results in Figures 2 through 11 for $B = 0$. The continuous linear shear model for the purely dissipative problem was solved by Barcilon [15], and his results are in good qualitative and approximate quantitative agreement with the two-layer model results.

For $B \neq 0$ and $E = 0$, the criterion equation (42) reduces to

$$B^2 = 2k^{*2}S\left(1 + \frac{1}{4}k^{*2}S\right)^2\left(1 - \frac{1}{8}k^{*2}S\right) \quad . \tag{49}$$

If one performs the preceding analysis with $E = 0$ from the beginning, a slightly different result is obtained, namely,

$$B^2 = k^{*4}S^2\left(1 - \frac{k^{*4}S^2}{64}\right) \quad . \tag{50}$$

The stability criteria equations (49) and (50) are plotted in Figure 14 as S versus B for different values of m. Note the small area in which equation (49) envelops equation (50). This means that a small amount of viscosity destabilizes the model in that area. This result was first obtained and discussed by Holopainen [11]. The finite amplitude aspects of this problem are discussed by Romea [16].

The continuous, inviscid, β-plane model was first presented by Charney [13]. Charney found a long wavelength cutoff, but later work [17,18] showed that this cutoff existed only in a limited sense. An up-to-date account of the continuous model results for linear and nonlinear shears is given by Geisler and Garcia [19].

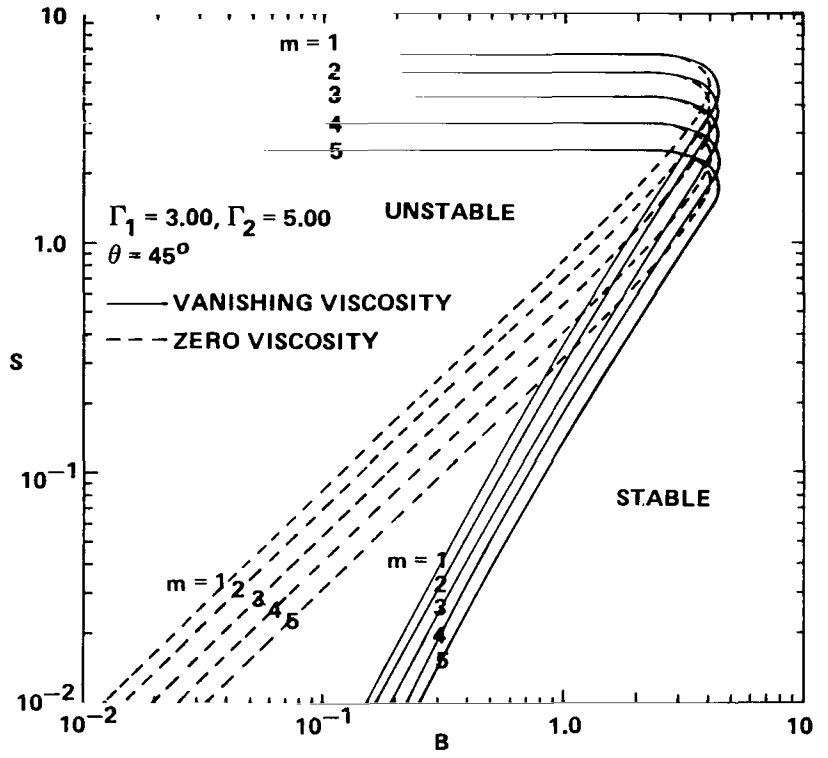

Figure 14. Plots of the inviscid, marginal stability curves as S versus B for different values of m and for the conditions of Figure 8 (Γ_1 = 3.00, Γ_2 = 5.00, B = 2.00) [the continuous curves are for vanishing viscosity, equation (49), and the dashed curves for zero viscosity, equation (50)].

REFERENCES

1. Hart, J. E.: Studies of Earth Simulation Experiments. NASA Contractor Report NASA CR-2753, NASA, Washington, D. C., 1976.

2. Fowlis, W. W. and Fichtl, G. H.: Geophysical Fluid Flow Model Experiments in Spherical Geometry. Proceedings of the Third NASA Weather and Climate Program Science Review. NASA Conference Publication 2029, Paper No. 32, 1977, p. 177.

3. Fultz, D., Owens, G. V., Bohan, W., Kaylor, R., and Weil, J.: Studies of Thermal Convection in a Rotating Cylinder with Some Implications for Large-Scale Atmospheric Motions. Meteor. Monog., 4, No. 21, 1959.

4. Hide, R.: An Experimental Study of Thermal Convection in a Rotating Liquid. Philos. Trans. Roy. Soc. Lond (A), 250, 1958, p. 441.

5. Fowlis, W. W. and Hide, R.: Thermal Convection in a Rotating Annulus of Liquid: Effect of Viscosity on the Transition Between Axisymmetric and Non-Axisymmetric Flow Regimes. J. Atmos. Sci., 22, 1965, p. 541.

6. Holton, J. R.: An Introduction to Dynamic Meteorology. International Geophysics Series, Academic Press, 1972.

7. Greenspan, H. P.: The Theory of Rotating Fluids. Cambridge University Press, Cambridge, 1969.

8. Pedlosky, J.: The Stability of Currents in the Atmosphere and the Ocean: Part I. J. Atmos. Sci., 21, 1964(a), p. 201.

9. Pedlosky, J.: The Stability of Currents in the Atmosphere and the Ocean: Part II. J. Atmos. Sci., 21, 1964(b), p. 342.

10. Bretherton, F. P.: Baroclinic Instability and the Short Wavelength Cut-Off in Terms of Potential Vorticity. Quart J. Roy. Met. Soc., 92, 1966, p. 335.

REFERENCES (Concluded)

11. Holopainen, E. O.: On the Effect of Friction in Baroclinic Waves. Tellus, 13, 1961, p. 363.

12. Lorenz, E. N.: The Nature and Theory of the General Circulation of the Atmosphere. Report of the WMO, 1967.

13. Charney, J. G.: The Dynamics of Long Waves in a Baroclinic Westerly Current. J. of Meteor., 4, 1947, p. 135.

14. Eady, E. T.: Long Waves and Cyclone Waves. Tellus, 1, 1949, p. 33.

15. Barcilon, V.: Role of the Ekman Layers in the Stability of the Symmetric Regime Obtained in a Rotating Annulus. J. Atmos Sci., 21, 1964, p. 291.

16. Romea, R. D.: The Effects of Friction and β on Finite-Amplitude Baroclinic Waves. J. Atmos. Sci., 34, 1977, p. 1689.

17. Green, J. S.: A Problem in Baroclinic Instability. Quart J. Roy. Met. Soc., 86, 1961, p. 237.

18. Burger, A. P.: On the Non-Existence of Critical Wavelengths in a Continuous Baroclinic Stability Problem. J. Atmos. Sci., 19, 1962, p. 31.

19. Geisler, J. E. and Garcia, R. R.: Baroclinic Instability at Long Wavelengths on a β-Plane. J. Atmos. Sci., 34, 1977, p. 311.

TECHNICAL REPORT STANDARD TITLE PAGE

1. REPORT NO.	2. GOVERNMENT ACCESSION NO.	3. RECIPIENT'S CATALOG NO.
NASA TP-1328		

4 TITLE AND SUBTITLE

The Effects of Curvature and Viscosity on Baroclinic Instability — A Two-Layer Model

5. REPORT DATE: September 1978

6. PERFORMING ORGANIZATION CODE

7. AUTHOR(S)

William W. Fowlis and Salvador Arias

8. PERFORMING ORGANIZATION REPORT #

9. PERFORMING ORGANIZATION NAME AND ADDRESS

George C. Marshall Space Flight Center
Marshall Space Flight Center, Alabama 35812

10. WORK UNIT NO.: M-264

11. CONTRACT OR GRANT NO.

12 SPONSORING AGENCY NAME AND ADDRESS

National Aeronautics and Space Administration
Washington, D.C. 20546

13. TYPE OF REPORT & PERIOD COVERED: Technical Paper

14. SPONSORING AGENCY CODE

15. SUPPLEMENTARY NOTES

Prepared by Space Sciences Laboratory, Science and Engineering

16. ABSTRACT

A linear stability analysis of a baroclinic zonal current contained between two parallel rigid boundaries is presented. Curvature is included by performing the analysis on a β-plane and viscosity by allowing for the effects of Ekman layers on the rigid boundaries. A two-layer model is used. This calculation was carried out to assist in the design of a spherical model of the general circulation of the Earth's atmosphere for Spacelab. In the low-gravity environment on an orbiting vehicle, a dominant radial dielectric body force, analogous to planetary gravity, can be achieved over a volume of liquid held between two concentric spheres. The results show the Eady short wavelength cutoff, and long wavelength cutoffs due to Ekman damping and curvature.

17. KEY WORDS

Baroclinic instability
Baroclinic modeling

18. DISTRIBUTION STATEMENT

Category 47

19. SECURITY CLASSIF. (of this report)	20. SECURITY CLASSIF. (of this page)	21. NO. OF PAGES	22. PRICE
Unclassified	Unclassified	31	$4.50

MSFC - Form 3292 (Rev Decemb

* For sale by the National Technical Information Service, Springfield, Virginia 22161

NASA-Langley, 1978

National Aeronautics and
Space Administration

Washington, D.C.
20546

Official Business
Penalty for Private Use, $300

THIRD-CLASS BULK RATE

Postage and Fees Paid
National Aeronautics and
Space Administration
NASA-451

U.S.MAIL

3 1 1U,E, 090178 S00903DS
DEPT OF THE AIR FORCE
AF WEAPONS LABORATORY
ATTN: TECHNICAL LIBRARY (SUL)
KIRTLAND AFB NM 87117

NASA

POSTMASTER: If Undeliverable (Section 158 Postal Manual) Do Not Return